Formation of wrinkles in outwardly propagating flames

M. Rahibe,[1,2] N. Aubry,[1,2] G. I. Sivashinsky,[1,3] and R. Lima[1,4]
[1]*The Benjamin Levich Institute, The City College of the City University of New York, New York, New York, 10031*
[2]*The Mechanical Engineering Department, The City College of the City University of New York, New York, New York, 10031*
[3]*School of Mathematical Sciences, Tel Aviv University, Ramat Aviv Tel Aviv 69978, Israel*
[4]*Centre de Physique Théorique, CNRS-Luminy, Case 907, 13288 Marseille Cedex 09, France*
(Received 17 March 1995)

Numerical integrations of the partial differential equation proposed by Filyand, Sivashinsky, and Frankel [Physica D 72, 110 (1994)] to describe the dynamics of outward accelerating flames are presented. The computational results reported by Filyand, Sivashinsky, and Frankel are confirmed: as time increases, a repetitive formation of cusps, as well as a rapid (power-law) expansion of the mean flame radius, are observed. However, the identification of invariant subspaces for the equation shows that even when the initial condition belongs to such subspaces, numerical round-off errors are responsible for excursions of the solution outside these subspaces. In Fourier space, this corresponds to the generation of spurious Fourier modes that grow as time increases. This computational error is controlled here by a filter that forces the solution, at each time step, to stay inside the invariant subspaces. The results of our filtered simulations are very similar to those resulting from unfiltered integrations, showing that both the formation of cusps and the rapid acceleration of the flame front are independent of the growth of spurious Fourier modes. The connection between such dynamics and exact pole solutions of the equation (in which the number of poles is fixed) is investigated. It is found that the latter are unstable and the more complicated (stable) dynamics consists of successive instabilities through which the flame front closely follows a $(2N+1)$-pole solution before approaching a $(2N+3)$-pole solution. These migrations are responsible for both the formation of new cusps and the rapid power-law acceleration of the mean front.

PACS number(s): 47.20.Ma, 82.40.Py, 47.20.Ky, 47.54.+r

I. INTRODUCTION

It was shown in [1] that, under a weakly nonlinear approximation, the dynamics of a cylindrical wrinkled flame front is governed by a nonlinear partial differential equation (PDE), which, in nondimensional variables, takes the form

$$\frac{\partial\Phi}{\partial\tau}-\frac{1}{2\bar{\Phi}^2}\left[\frac{\partial\Phi}{\partial\theta}\right]^2=\frac{1}{\bar{\Phi}^2}\frac{\partial^2\Phi}{\partial\theta^2}+\frac{\gamma}{2\bar{\Phi}}I\{\Phi\}+1\ . \quad (1)$$

Here, Φ is the nondimensional interface of the perturbed circular flame, $\Phi=U_bD_M^{-1}R$, τ is the nondimensional time, $\tau=\gamma^2U_b^2D_M^{-1}t$, and θ is the angular position $(0\le\theta\le2\pi)$. In these expressions, U_b is the normal speed of a planar flame relative to the burning gas, D_M is the Markstein diffusivity and γ is the thermal expansion coefficient. The overbar denotes the average over θ, i.e.,

$$\bar{\Phi}(\tau)=\frac{1}{2\pi}\int_0^{2\pi}\Phi(\theta,\tau)d\theta\ . \quad (2)$$

$I\{\ \}$ represents a linear singular nonlocal operator which is responsible for the Darrieus-Landau instability [2,3]. It has the two following formal representations:

$$I\{\Phi\}=\frac{1}{\pi}\sum_{m=1}^{\infty}m\int_0^{2\pi}\cos[m(\theta-\vartheta)]\Phi(\vartheta,\tau)d\vartheta \quad (3)$$

and

$$I\{\exp(im\theta)\}=|m|\exp(im\theta) \quad (4)$$

in Fourier space.

The numerical integrations of the PDE (1) performed in [1], as well as those presented in Sec. V of this paper, show a qualitative agreement with various experimental results reported in [4]. In particular, cusps are formed on the interface, which becomes more and more wrinkled as time increases. As wrinkles develop, the expansion of the wrinkled front accelerates, and the (azimuthal) mean radius seems to increase with time according to a $\tau^{3/2}$ power law. In addition, wrinkles have their own dynamics: their shape and angular location change with time. This repetitive formation of cusps as time increases has been interpreted as a self-fractalization process based on a renormalization picture of the front wrinkling [4].

A PDE structurally similar to (1) was studied by Joulin [5] for expanding circular flame fronts. By using a pole decomposition method (see [5,6], and references therein), Joulin reduced the PDE to a finite set of ordinary differential equations (ODE) describing the motion of the poles in the complex plane. The shape of the flame front obtained from *these particular solutions* can then be deduced from the knowledge of the position of the poles at each time τ. However, numerical and analytical results show that the solutions of the ODEs do not resemble those obtained from the numerical integration of the original PDE. In particular, the number of wrinkles obtained from the ODEs is independent of time and the corresponding (mean) expansion of the front is much slower than the $\tau^{3/2}$ power law. For instance, in the case of the one-pole solution (see its expression in Sec. II below), the front grows linearly with time asymptotically and the an-

gular position of the wrinkles is fixed. It was then suggested [5,6] that nonlinearity alone is not enough to mimic the experimental observations and that the results of the spectral numerical integrations of [1] may be due to computational noise. These conclusions led to the derivation of another model [6], where pseudorandom external forcing is included. In this case, it is shown that many broad-banded exciting fields indeed lead to the rapid spawning of wrinkles.

In this paper, we return to the PDE (1) without external forcing. From a pole decomposition of the solutions, we derive exact solutions of the PDE and numerically integrate the set of ODEs thus obtained. We confirm the results of [5] that these solutions are fundamentally different from the experimental observations. This, however, is not too surprising to us since, in this approach, the number of poles is fixed *by assumption.* Therefore, while this method is extremely attractive for giving access to exact solutions of the PDE, it does not address the question of the stability of such solutions *for the PDE itself.* At this point, two questions need to be addressed.

(i) Are the solutions built with a fixed number of poles stable for the PDE?

(ii) Are there stable solutions for the PDE that allow the formation of new poles as time increases?

In other words, are the formation of the new wrinkles and the fast acceleration of the flame front due to numerical artifacts or, instead, are they intrinsic to the dynamics of the PDE?

In this paper, we investigate the origin of the discrepancy between the numerically obtained solution of the PDE and the solutions of the set of ODEs. We perform numerical simulations of the PDE by filtering various (but not all) sources of computational errors and obtain results that support both the generation of wrinkles and the power law for the acceleration of the mean flame front. These findings indicate that the discrepancy between the solution of the set of ODEs and the numerically obtained solution of the PDE originates in the fact that the functions containing a fixed number of poles are unstable solutions of the PDE. Consequently, they are not observed in most numerical integrations and physical experiments.

The paper is organized as follows. In Sec. II, we apply a pole decomposition method to derive exact solutions of the PDE (1) as well as the set of ODEs they satisfy. We also give an analytical expression of the Fourier spectra of such solutions. In Sec. III, we show that the PDE has two invariant subspaces which we use in devising a noise control procedure for the numerical integrations. We present our numerical scheme in Sec. IV and integrate both the PDE and the previous set of ODEs in Sec. V. This is performed by using the same initial condition consisting of one pole. We show that the role of the noise outside the previous invariant subspaces is minor; in both the unfiltered and filtered computations, the solution of the PDE stays close to a configuration with $2N+1$ poles before approaching a $2N+3$-pole solution, as is particularly clear in Fourier space. The process keeps repeating itself as time increases. We then conclude in the last section.

II. EXACT SOLUTIONS

For the sake of simplicity, we introduce the function $\Psi(\theta,\tau)$ which is related to the front $\Phi(\theta,\tau)$ by the relation $\Phi(\theta,\tau)=\tau+\Psi(\theta,\tau)$. From Eq. (1), it is straightforward to derive the PDE satisfied by $\Psi(\theta,\tau)$,

$$\frac{\partial\Psi}{\partial\tau}-\frac{1}{2\bar{\Phi}^2}\left[\frac{\partial\Psi}{\partial\theta}\right]^2=\frac{1}{\bar{\Phi}^2}\frac{\partial^2\Psi}{\partial\theta^2}+\frac{\gamma}{2\bar{\Phi}}I\{\Psi\}\ . \tag{5}$$

We now apply a pole decomposition technique, assuming that the function

$$\Psi_k(\theta,\tau)=2\sum_{\alpha=1}^{2N}\ln\left[\sin\left[\frac{k\theta-Z_\alpha(\tau)}{2}\right]\right]+f_k(\tau) \tag{6}$$

is a solution of (5). The time dependent Z_α's are poles of $\Psi(\theta,\tau)$ in the complex plane and they appear in complex conjugate pairs. Their dynamics is governed by the following system of ODEs:

$$\dot{Z}_\alpha(\tau)=-\frac{k^2}{\bar{\Phi}^2}\sum_{\alpha\neq\beta}\cot\left[\frac{Z_\alpha-Z_\beta}{2}\right]-i\frac{\gamma k}{2\bar{\Phi}}\mathrm{sgn}(\mathrm{Im}Z_\alpha)\ , \tag{7}$$

where Im denotes the imaginary part and the function sgn has the usual meaning, namely, $\mathrm{sgn}(0)=0$ and $\mathrm{sgn}(x)=|x|/x$ if $x\neq0$. Here $\bar{\Phi}(\tau)$ is related to $f(\tau)$, whose dynamics is deduced from the azimuthal average of (5), i.e.,

$$\frac{d\bar{\Psi}(\tau)}{d\tau}=\frac{1}{\bar{\Phi}^2}\overline{(\Psi_\theta)^2}\ .$$

For a pole solution (6), the number of cusps $\mathcal{N}$ is smaller than or equal to $\mathcal{N}\leq kN$, where k is an integer.

For the following, it is useful to rewrite Eq. (6) by using elementary mathematical functions with real arguments. We thus decompose $Z_\alpha(\tau)=a_\alpha(\tau)+ib_\alpha(\tau)$, which, after substitution in (6), leads to

$$\Psi_k(\theta,\tau)=2\sum_{\alpha=1}^{N}\ln\tfrac{1}{2}\{\cosh b_\alpha(\tau)-\cos[k\theta+a_\alpha(\tau)]\}+f_k(\tau)\ . \tag{8}$$

A more general expression can be constructed by summing, over various k's, two or more functions Ψ_k given by (6) [or (8)]. Despite the nonlinearity of the PDE, this new function is another solution of the PDE (5). However, the laws of motion of the poles must be rewritten in this case, particularly because the poles interact, due to the action of the nonlinear terms.

For the simplest solution defined with one pole and its conjugate $[Z(\tau)=a(\tau)\pm ib(\tau)]$, the dynamics takes the simple form

$$\begin{aligned}\dot{a}&=0\ ,\\ \dot{b}&=\frac{k^2}{\bar{\Phi}^2}\coth[b(\tau)]-\frac{\gamma k}{2\bar{\Phi}}\ ,\\ \dot{f}&=\frac{\gamma k}{\bar{\Phi}}-\frac{2k^2}{\bar{\Phi}^2}\ .\end{aligned} \tag{9}$$

The angular position of the wrinkles is therefore fixed, as the angle values $\theta_i = a(\tau_0) + (2\pi/k)i, 0 \le i \le k-1$, where $a(\tau_0)$ is constant. The set of ODEs, in this case, reduces to a unique equation for b and the shape of the flame front is given by

$$\Psi(\theta,\tau) = 2\ln\tfrac{1}{2}[\cosh b(\tau) - \cos(k\theta)] + f(\tau) . \tag{10}$$

For these solutions, the mean radius of the flame front, or the zero Fourier mode, $\hat{\Phi}_0(\tau)$, of $\Phi(\theta,\tau)$, is obtained as a function of $b(\tau)$:

$$\bar{\Phi}(\tau) = \hat{\Phi}_0(\tau) = \tau + 2b(\tau) - 4\ln 2 + f(\tau) . \tag{11}$$

The other Fourier modes ($m \neq 0$) of $\Psi(\theta,\tau)$ are computed by means of the method of residues, leading to the equations

$$\hat{\Psi}_m(\tau) = \begin{cases} -\dfrac{2e^{-nb(\tau)}}{n} & \text{if } m = nk \\ 0 \quad \text{otherwise} . \end{cases} \tag{12}$$

It is then straightforward to see that the Fourier coefficients of the flame front $\hat{\Phi}_m$ are equal to those of $\Psi(\theta,\tau)$, for all nonzero Fourier modes.

We now consider a particular subset of solutions of the form (8), those given by the space-time functions

$$\begin{aligned} \Psi(\theta,\tau) = {} & 2\ln\tfrac{1}{2}[\cosh b(\tau) - \cos k\theta] \\ & + 2\sum_{j=1}^{N} \ln\tfrac{1}{2}\{\cosh b_j(\tau) - \cos[k\theta + a_j(\tau)]\} \\ & + 2\sum_{j=1}^{N} \ln\tfrac{1}{2}\{\cosh b_j(\tau) - \cos[k\theta - a_j(\tau)]\} \\ & + f(\tau) . \end{aligned} \tag{13}$$

For these solutions, the mean radius, or the zero Fourier mode, is given by the expression

$$\begin{aligned} \bar{\Phi}(\tau) = \hat{\Phi}_0(\tau) = {} & \tau - (2+2N)\ln 4 + 2b(\tau) \\ & + 4\sum_{j=1}^{N} b_j(\tau) + f(\tau) , \end{aligned} \tag{14}$$

while the other Fourier modes ($m \neq 0$) are

$$\hat{\Phi}_m(\tau) = \begin{cases} -\dfrac{2e^{-nb(\tau)}}{n} - 4\displaystyle\sum_{j=1}^{N} \frac{e^{-nb_j(\tau)}}{n} \cos n a_j(\tau) & \text{if } m = nk \\ 0 \quad \text{otherwise} . \end{cases} \tag{15}$$

It is straightforward to deduce the Fourier transforms (14) and (15) from the more general expressions (11) and (12), using the fact that the Fourier transform is a linear operator.

It is interesting to note that the one-pole solution (10) and the $(2N+1)$-pole solution (13) have common properties: they are both even functions of θ (namely, invariant under the reflection symmetry $\theta \to -\theta$) and periodic, of period $2\pi/k$ (or $2\pi/n_0 k$, where $n_0 k$ is the first wave number with nonzero Fourier coefficient) at all times. In other words, their Fourier transforms are real functions and the only nonzero Fourier coefficients correspond to the wave number k and its harmonics. The more general N-pole solutions (8) enjoy the latter property, but not the former.

The previous pole decomposition is similar to that used by Thual, Frish, and Henon [7], who have applied such a procedure to the Michelson-Sivashinsky equation [8] (see also Joulin and Cambray [9] and Renardy [10]). The N-pole solutions (6) are also found by Joulin [5] and Minaev [11], who used a slightly different method.

III. INVARIANT SUBSPACES FOR THE PDE

In the preceding section, we have mentioned that both the one-pole solutions (10) and the $(2N+1)$-pole solutions (13) have a real Fourier transform which takes nonzero values only for the wave number k and its harmonics. We now show that such properties are constants of motion for the PDE (1). Indeed, if one of these two properties holds *initially*, then it holds *at all times*. More precisely, (a) if, at the initial time τ_0, the Fourier transform of $\Phi(\theta,\tau_0)$ is real, then at any time $\tau \ge \tau_0$, $\Phi(\theta,\tau)$ has also a real Fourier transform; (b) if, at the initial time τ_0, $\Phi(\theta,\tau_0)$ has all its Fourier coefficients $\hat{\Phi}_m(\tau_0) = 0$ for all integers m such that, for a given integer k, m/k is not an integer, then $\Phi(\theta,\tau)$, for $\tau \ge \tau_0$, enjoys the same property.

Equivalently, we say that the set of real functions in $[0,2\pi]$, whose Fourier transform is real, Σ_1, and the set of real solutions in $[0,2\pi]$ whose Fourier coefficients are nonzero only for one wave number k and its harmonics, Σ_2, are two invariant subspaces for the PDE (1).

Properties (a) and (b) above can be easily shown by substituting the Fourier transform of $\Phi(\theta,\tau)$, i.e.,

$$\Phi(\theta,\tau) = \sum_{m=-\infty}^{m=+\infty} \hat{\Phi}_m(\tau) \exp(ik\theta) \tag{16}$$

in (1). This leads to the system of ODEs

$$\begin{aligned} \frac{d\hat{\Phi}_m(\tau)}{d\tau} + \frac{1}{2\bar{\Phi}^2} \sum_{p+q=m} pq\hat{\Phi}_p(\tau)\hat{\Phi}_q(\tau) \\ = -\frac{1}{\bar{\Phi}^2} m^2 \hat{\Phi}_m(\tau) + \frac{|k|\gamma}{2\bar{\Phi}} \Phi_m(\tau) \end{aligned} \tag{17}$$

and

$$\frac{d\hat{\Phi}_0(\tau)}{d\tau} = \frac{1}{2\bar{\Phi}^2} \sum_{m \neq 0} m^2 |\hat{\Phi}_m(\tau)|^2 . \tag{18}$$

Properties (a) and (b) can then be deduced in a straightforward manner.

The consideration of the two previous invariant subspaces can be very useful in studying the role played by numerical noise. As is well known, avoiding roundoff errors in numerical computations is a difficult task. For instance, such errors often prevent us from obtaining zero after simple arithmetic operations, even when the analytical result is zero. In this case, the value given by the computer depends on the arithmetic precision. In the present study, such an effect can be observed in the simple computation of the Fourier transform of a one-pole solution (10). In the example shown in Fig. 1(a), parameters b and k have been set to the values $b=1.0$ and $k=4$. Figure 1(b) displays its Fourier transform numerically computed by using a standard fast Fourier transform (FFT) algorithm. While it is clear that the computed Fourier amplitudes, above the level of the numerical noise, coincide with the expression (12) for the wave number k and its harmonics, spurious nonzero amplitudes appear at the level of roundoff errors for nonharmonic modes. In addition, high harmonic wave numbers

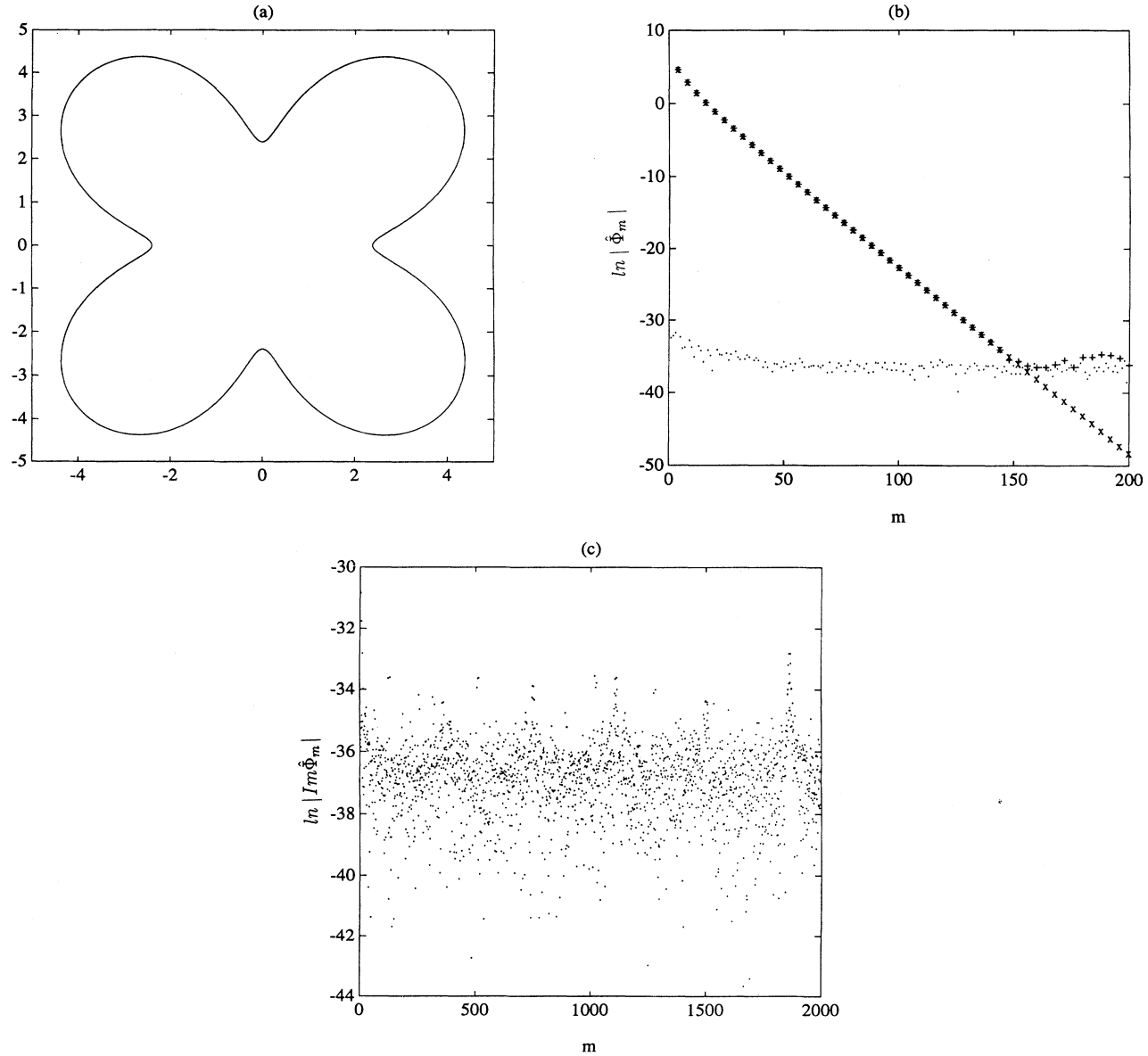

FIG. 1. The initial flame front consisting of one pole [see expression (10) in the text]. Here, as in all subsequent figures, the represented flame front is always normalized with the azimuthal mean radius, i.e., $\phi(\theta,\tau)/\bar{\phi}(\tau)$. The distance to the real axis is $b=1.0$: (a) the flame front itself; (b) the amplitude of the Fourier coefficients of the initial front: (x) values computed from the analytical expression (12) in the text; (+) and (·) values computed using a standard FFT [(+) corresponds to the amplitude of the principal modes and (·) corresponds to the appearance of spurious coefficients]; (c) the imaginary part of the Fourier coefficients of the initial front computed using a standard FFT.

for which the Fourier amplitude should be below the noise level according to the analytical expression (12) have an artificially high amplitude. Similarly, Fig. 1(c) shows the imaginary part of the Fourier coefficients corresponding to harmonic wave numbers. It is clear that while such modes should be identically zero, the numerical computation gives nonzero values.

Although the previous computation has nothing to do, *a priori,* with the integration of the equation of motion (1), it indicates that the invariance properties (a) and (b) of the latter will not be satisfied through numerical integrations unless some special care is taken. This remark is particularly valid for the specific solutions of the PDE (1) which, at any given time, can be written as a superposition of poles (13). The effect of this artificial excursion of the solution away from the invariant subspaces is not known and deserves attention. In the next section, we thus concentrate on numerical simulations for which the initial condition lies in the invariant subspace $\sum_1 \cap \sum_2$. We then perform simulations with and without noise control. In the former experiments, we impose that the solution stay in the invariant subspace $\sum_1 \cap \sum_2$ *at each time* by systematically setting all spurious Fourier amplitudes to zero. In addition, we set all Fourier coefficients smaller, in absolute value, than a certain threshold to zero, as in the filter used in [12].

IV. NUMERICAL SCHEME

We have performed numerical integration of (1) by using the algorithm used in [1] consisting of a Fourier pseudospectral procedure supplemented by the slaved-frog method for the advancement in time (proposed and used in [7]). The only differences between our algorithm and that used in [1] lie in the fact that we use a high number of Fourier modes from the initial stage of the computation and we do not increase this number as time evolves. In addition, we apply the filter described in Sec. III in some integrations.

The iterative process, used to compute the shape of the flame front at $\tau+\delta\tau$ from the known shape at time τ, is given by the equation

$$\hat{\Phi}_m(\tau+\delta\tau)=\hat{\Phi}_m(\tau-\delta\tau)\exp[2\omega(m,\tau)\delta\tau] + \frac{\hat{G}_m(\tau)}{\omega(m,\tau)}\{1-\exp[2\omega(m,\tau)\delta\tau]\}\ , \tag{19}$$

where

$$\omega(m,\tau)=\frac{1}{2}\frac{\gamma m}{\overline{\Phi}(\tau)}-\left[\frac{m}{\overline{\Phi}(\tau)}\right]^2 . \tag{20}$$

Here $\hat{\Phi}_m(\tau)$ denotes the mth Fourier coefficient of $\Phi(\theta,\tau)$ and $\hat{G}_m(\tau)$ refers to the mth Fourier mode of the function $G(\theta,\tau)=\frac{1}{2}[\Phi_\theta/\overline{\Phi}(\tau)]^2+1$. In Eq. (19), the amplitude of all Fourier modes (except for $m=0$ and $m=N/2$) is, in general, a complex number.

The total number of modes is fixed to $N=16\,384$ in all the numerical simulations reported here, and the time step used is $\delta\tau=0.01$. The implementation of a time step twice smaller than this value does not affect the results presented in this paper. The integration is performed over the time intervals $\tau_0=5\le\tau\le\tau_{\max}=2000-4000$. This integration time and the number of Fourier modes N are chosen to meet the criterion $N>2.5\gamma\overline{\Phi}(\tau)$ at each time τ, as in [1]; this relation guarantees a good description of the interface in Fourier space. The initial condition is a one-pole solution given by the discretization of the function $\Phi(\theta,\tau_0)=\tau_0+\Psi(\theta,\tau_0)$, where $\Psi(\theta,\tau_0)$ satisfies (10) with $b(\tau_0)=1$. All our computations are performed in double precision.

In the simulations where the noise control is turned on, not only do we impose that the solution remain in the invariant subspace, but also we set the Fourier amplitudes which are smaller, in absolute value, than a certain threshold value, to zero, as in [12]. The selection of an appropriate threshold depends on the precision of the computation. Since we use double precision, we set the threshold to 10^{-28} in logarithmic scale, i.e., $\log|\hat{\Phi}_n|<-28$. It is clear that this filtering technique does not permit the control of round-off errors on nonzero values inside the invariant subspaces.

V. NUMERICAL EXPERIMENTS

In all our computations, the thermal expansion coefficient is fixed to the value used in [1], i.e., $\gamma=0.8$. For this fixed parameter value, we first integrate the PDE (1) without any particular filter. We recall here that our initial condition, displayed in Fig. 1(a), consists of four cusps whose numerically computed Fourier spectrum is shown in Fig. 1(b). As the integration progresses, the flame front evolves in a self-similar manner which manifests itself in the formation of cusps on the interface. This self-similarity is in a space-time sense: the number of cusps keeps growing as time increases. Such a repetitive creation of new cusps on the flame front leads to a small scale wrinkled interface as shown in Fig. 2(a), consistent with the earlier findings of [1]. This picture will be compared later with that obtained with the filtered computation [Fig. 2(b)]. Figure 3 gives some insight into this phenomenon in Fourier space. There, one clearly observes that the Fourier spectrum corresponding to the initial four cusp interface of Fig. 1 undergoes a local kink at about time $\tau=719$. Such a kink, occurring in the amplitude of the Fourier modes $k=4$ and its harmonics, is followed by an oscillation of this amplitude [Fig. 4(a)], which corresponds, in physical space, to the birth of four pairs of wrinkles. Figure 4(b) shows that the two wrinkles in each new pair emerge at symmetric positions on both sides of each initial cusp. This symmetry, characteristic of the invariant subspace $\sum_1$, persists at all subsequent times. This first instability is followed by a second one through which a second frequency appears in the oscillation of the Fourier amplitudes, a phenomenon which can be observed in Figs. 4(c) and 4(e). This second deformation, apparent at $\tau=863$, corresponds, in physical space, to the symmetric formation of pairs of new cusps on both sides of the previously generated cusps [see Figs. 4(d) and 4(f)]. The process, which keeps repeating itself (in the same symmetric manner), is responsible for the flame fractalization and the highly wrinkled structure of

the interface after some time. As time evolves, the generation of cusps is not the only phenomenon which takes place: there is a rich dynamics of the wrinkles consisting of both a deformation of their shape and a motion in the azimuthal direction. Meanwhile, the mean (fluctuating) front accelerates at a rate consistent with a $\tau^{3/2}$ power law.

It is difficult, *a priori,* to estimate the effect of the spurious amplitudes on the dynamics of the active Fourier mode k and its harmonics, and vice versa. During the events previously described, the amplitude of the spurious wave numbers increases. It also becomes very structured, mimicking the behavior of the active modes. Local kinks and oscillations, for instance, can be clearly observed in the spurious real part of the Fourier spectrum after the first instability [see, e.g., Fig. 4(c)]. The triggering kink described above, however, seems to appear among the mode k and its harmonics first, indicating that the latter are responsible for the instability. In any case, the dynamics of these active modes greatly influences the behavior of the spurious ones. We then apply the noise filter described in Sec. III and reiterate our numerical experiments with the same initial condition.

The filtered simulations give the same picture as the original numerical integrations. The one-pole solution (10) is found to be unstable, and new symmetric wrinkles appear on both sides of each original cusp. A more detailed comparison can be achieved by examining Figs. 4 and 5 which show that the first and second instabilities occur at about the same time in both simulations. In addition, after a rather long time, $\tau=7668$, for instance, the number of cusps that have formed on the interface is similar in both simulations [see Figs. 2(a) and 2(b)]. Such generation of wrinkles keeps occurring as time increases. These results indicate that the generation of new cusps is intrinsic to the dynamics of the mode k and its harmonics, rather than being due to the small amplitude numerical noise developing among nonharmonic modes when no filter is applied.

We now investigate the connection between the solution obtained in our filtered numerical integrations and the exact pole solutions of Sec. II. For this purpose, we first recall that the filter numerically applied is equivalent to forcing the dynamics to remain in the invariant subspace $\Sigma_1 \cap \Sigma_2$ defined in Sec. III. In this subspace, two good candidates for the front flame shape are given by $\Phi(\tau)=\tau+\Psi(\tau)$, where $\Psi(\tau)$ satisfies Eq. (13) with $N=1$ and $N=2$. From their analytical Fourier transforms (15), we know that these functions have an oscillating

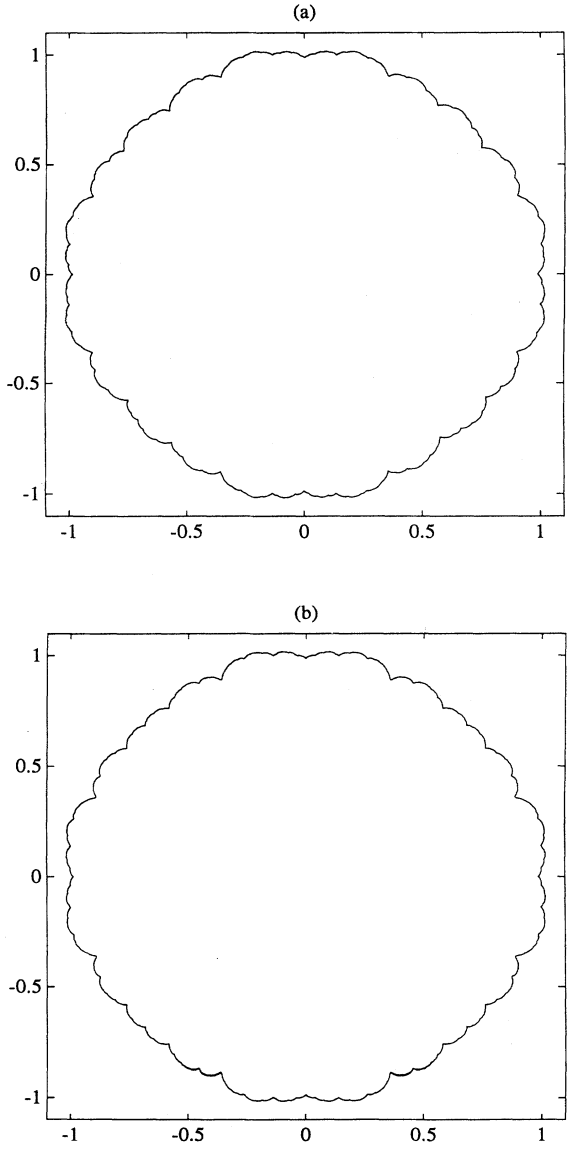

FIG. 2. The flame front computed by the numerical simulation of Eq. (1): (a) flame front at time $\tau=7668$ from the unfiltered computation; (b) flame front at time $\tau=7668$ from the filtered computation.

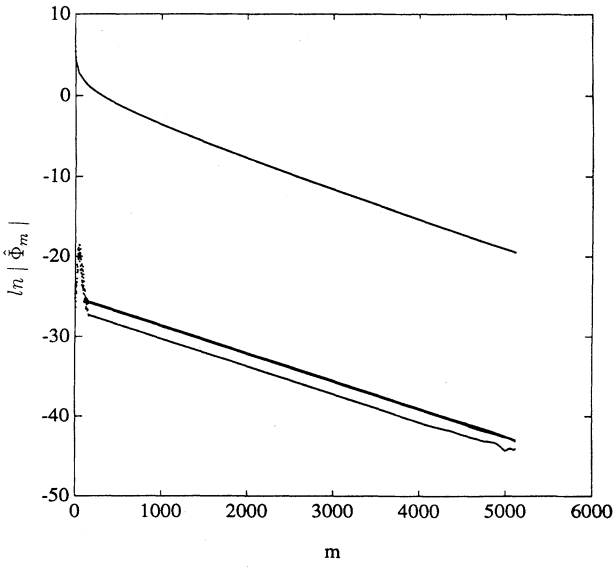

FIG. 3. The amplitude of the Fourier coefficients of the flame front at time $\tau=719$ obtained in the unfiltered computation showing the onset of the first instability.

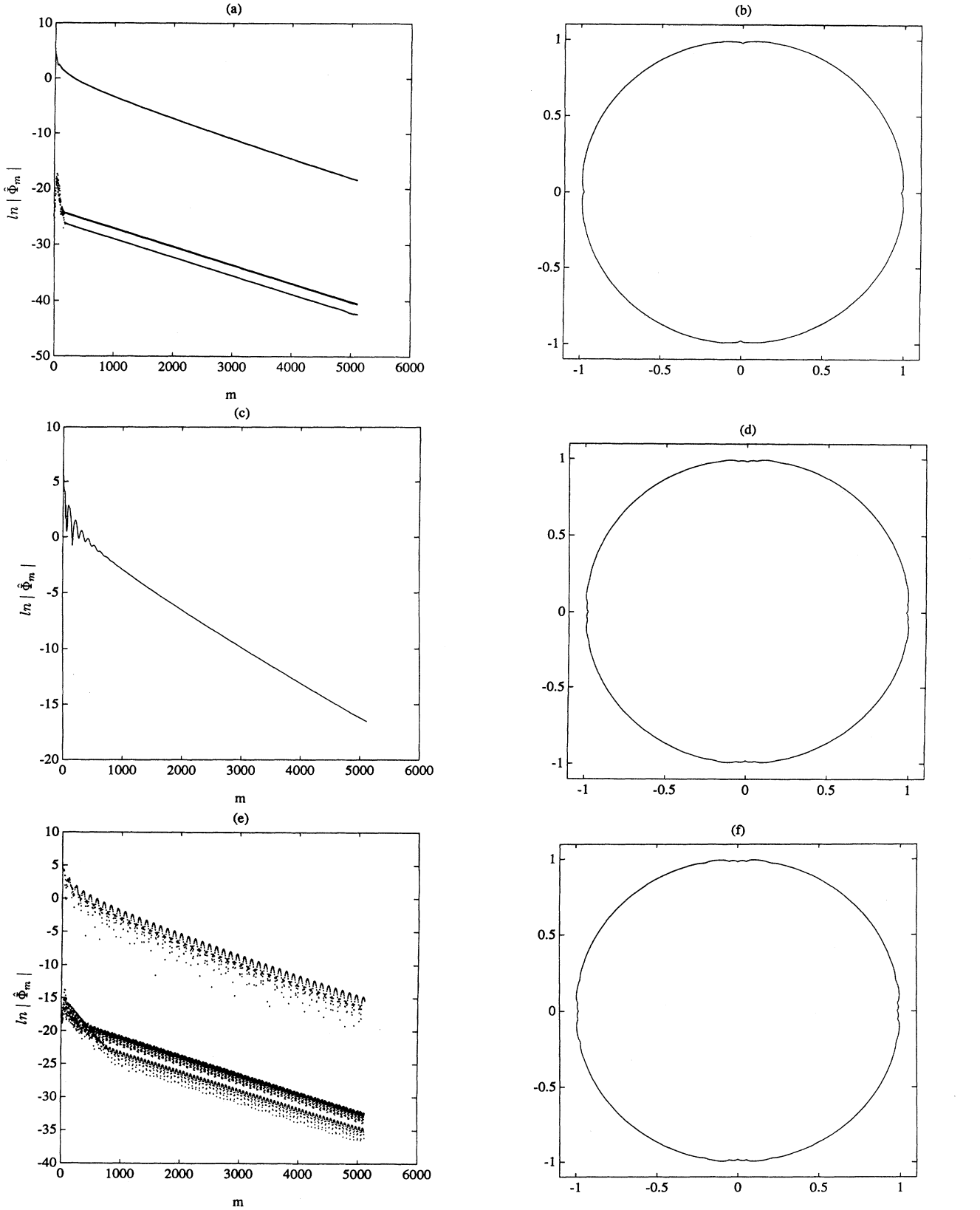

FIG. 4. The evolution of the solution obtained from the unfiltered simulation of Eq. (1) as time evolves showing the two first instabilities at times $\tau=767$, 863, 910: (a), (c), (e) show the evolution of the amplitude of the Fourier coefficients, and (b), (d), (f) show the formation of new cusps in the flame front.

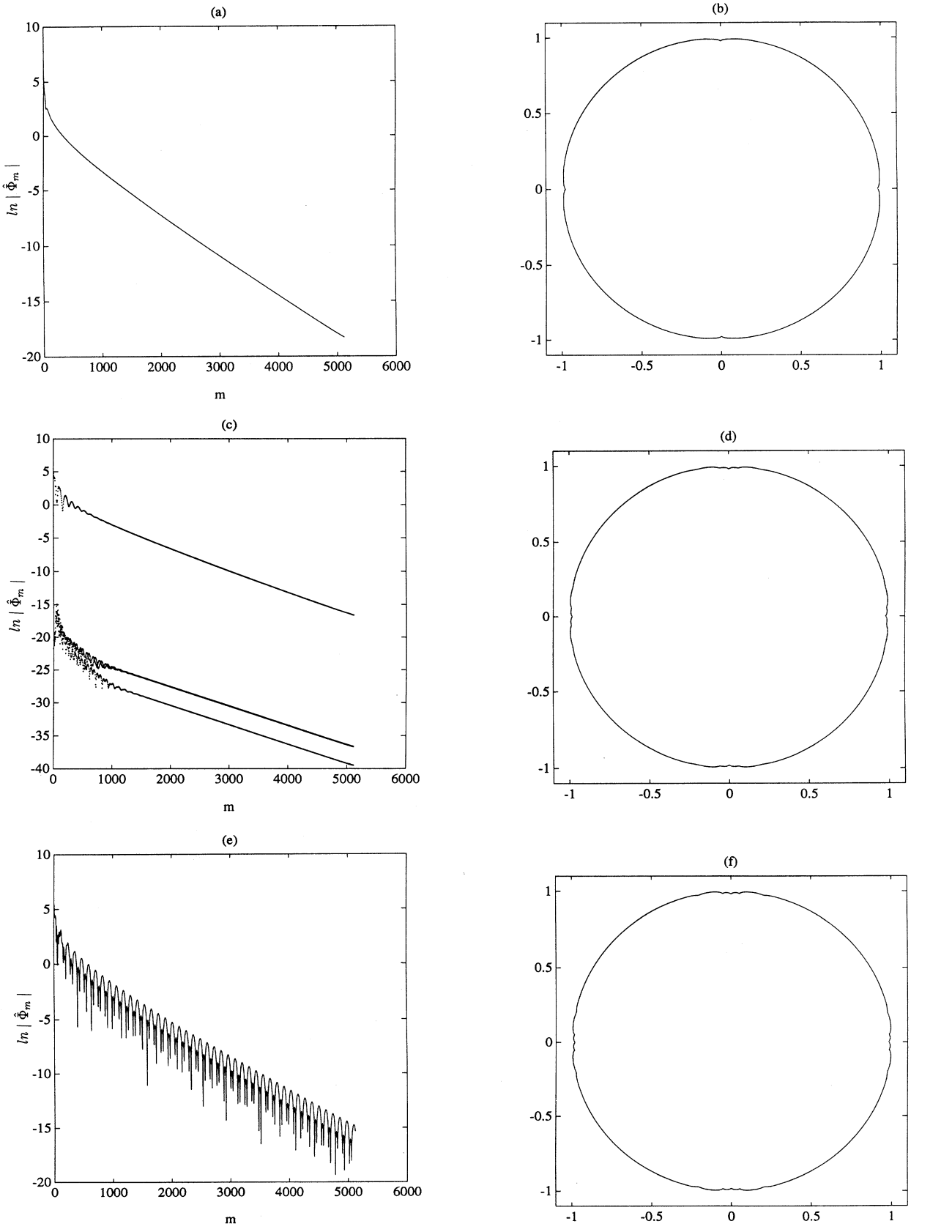

FIG. 5. The same as in Fig. 4 with the filtering procedure described in Sec. IV.

Fourier spectrum and their shape in physical space exhibits its symmetric wrinkles around the original cusps located at the angular positions $\theta=0,\pi/2,\pi,3\pi/2$. The results of our numerical simulations displayed in both the physical space and the Fourier space indicate that the numerical solution strongly resembles the analytical expression (13) with $n=1$ after the first instability onset, and $n=2$ after the second instability has occurred, as we explain below.

After a transient time, the solutions obtained with and without filter are consistent with a $\tau^{3/2}$ power law for the acceleration of the mean radius. More precisely, the (azimuthal) mean of the function $\Psi(\theta,\tau)$, that is, $\overline{\Psi}(\tau)=(1/2\pi)\int_0^{2\pi}\Psi(\theta,\tau)d\theta$, is increasing according to a $\tau^{3/2}$ power law (see also [1]). For large times, if this law persists, the term $\overline{\Psi}(\tau)$ will overcome the linear growth and therefore dominate in the expression of $\overline{\Phi}(\tau)$. Consequently, the latter will exhibit a $\tau^{3/2}$ power law as well (see Fig. 6 for this tendency in our numerical simulation at relatively early times). It is clear that both theoretical investigations and well resolved numerical integrations on longer time intervals are needed to confirm this scaling behavior. This point, however, is beyond the scope of the present paper.

We have also performed numerical integrations of the ODEs (9) with the same one-pole initial condition as for the PDE. These integrations are performed using a Runge-Kutta-Merson method [13] over a full time interval $\tau\in[5,4000]$ successively divided into small intervals of duration $\delta\tau=0.1$. Since the number of poles here is fixed by construction, we do not observe the creation of new poles or cusps. As found numerically and analytically in [5], the distance of the pole to the real axis, $b(\tau)$, asymptotically decreases proportionally to $1/\tau$ in this solution. The corresponding mean radius increases linearly with time asymptotically $[\overline{\Phi}(\tau)\propto\tau]$ and therefore, no accelerating component is present. Our aim, however, in performing this simulation, is to compare such a solution with that obtained from the PDE (1) before the occurrence of the first instability. In Fig. 7, we carry out such comparison between the solution of the ODE (9) and the results obtained from both the unfiltered and filtered integrations of the PDE (1). Assuming that the solution of the latter is close to a pole solution, we extract $b(\tau)$ from the numerically computed Fourier spectrum and Eq. (12) with $n=1$ and $n=2$. Both curves thus obtained coincide, up to the time where the one-pole solution becomes unstable (see Fig. 7). In addition, a comparison between Figs. 7(a) and 7(b) and Figs. 7(c) and 7(d) shows that the presence of the spurious Fourier modes does not have much influence on this first part of the integration. (Although the previous extraction technique is no longer formally valid in presence of noise in the imaginary part of the Fourier spectrum, we still use it as a reference criterion in unfiltered simulations.) While the extracted $b(\tau)$ first increases, it then decreases. This decrease becomes linear in $1/\tau$ just before the occurrence of the instability, reproducing, in this finite time interval, the asymptotic behavior provided by the ODE. A more precise comparison between the ODE and the PDE dynamics is performed in Fig. 8.

Similarly, Fig. 9 displays the Fourier spectrum of the three-pole (symmetric) solution (13) with $N=2$, $a_1=0.2$, $a_2=0.31$, $b=b_1=0.01$, and $b_2=0.02$. We recall that Fig. 5(e) shows the solution of the PDE (1) right after the second pairs of cusps have appeared. The similarity between the two figures indicates that Eq. (13) is a good description of the flame front obtained from the PDE after the second instability and before the third one. (The slight discrepancies that can be observed should vanish as the parameters of the three-pole solution are better adjusted.) A qualitative comparison of the solution of the PDE (1) in a time interval between the Nth instability and

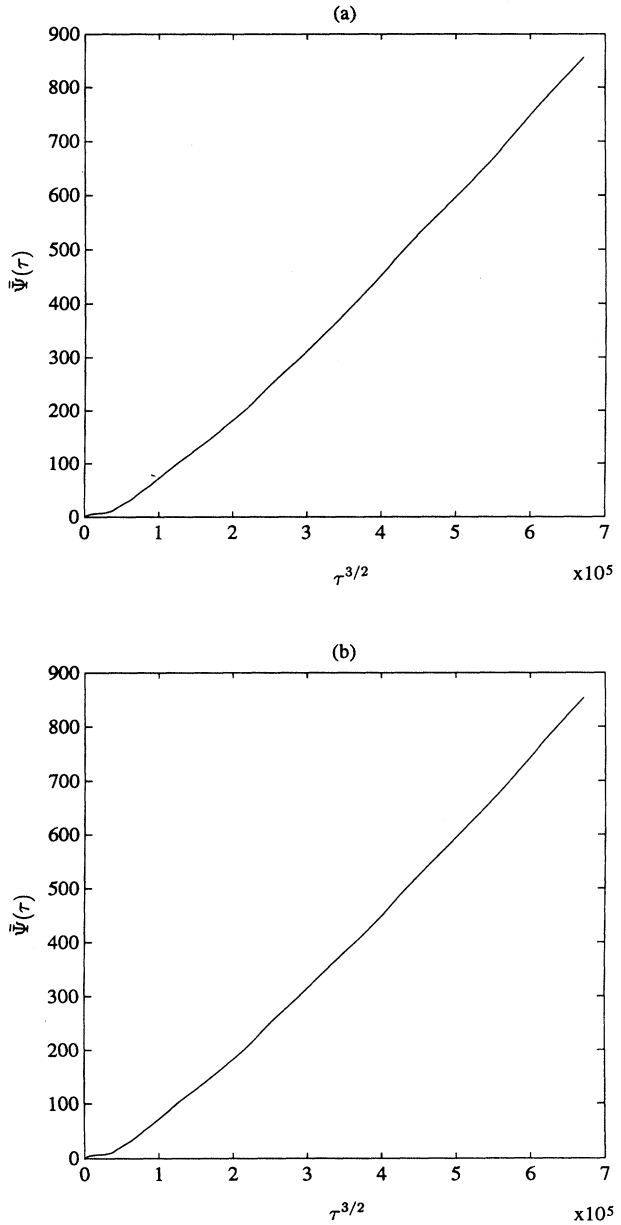

FIG. 6. The growth of the azimuthal average of the fluctuation Ψ as a function of $\tau^{3/2}$: (a) obtained with the unfiltered simulation; (b) obtained with the filtered simulation of Eq. (1).

the $(N+1)$th instability indicates that the $(2N+1)$-pole solution (13) remains a good model during this time interval.

VI. CONCLUDING REMARKS

The study performed in this paper confirms that the model derived in [1] for the outward propagating spherical flame in the regime of well developed hydrodynamic instability leads to the self-fractalization of the flame front. This mechanism consists of successive instabilities through which cusps are born: the interface becomes more and more wrinkled as time increases. Computational round-off errors in the integration of the PDE are, however, found to be responsible for the birth and growth of spurious Fourier modes in the solution. When the latter are filtered, which is equivalent to maintaining the solution in well defined invariant subspaces, self-fractalization persists. Nevertheless, this behavior is fundamentally different from exact pole-solutions for which the number of poles (and cusps) is constant. It has been shown in [5], and confirmed in this paper, that such poles asymptotically approach the real axis, a phenomenon which is inconsistent with the faster expansion of the

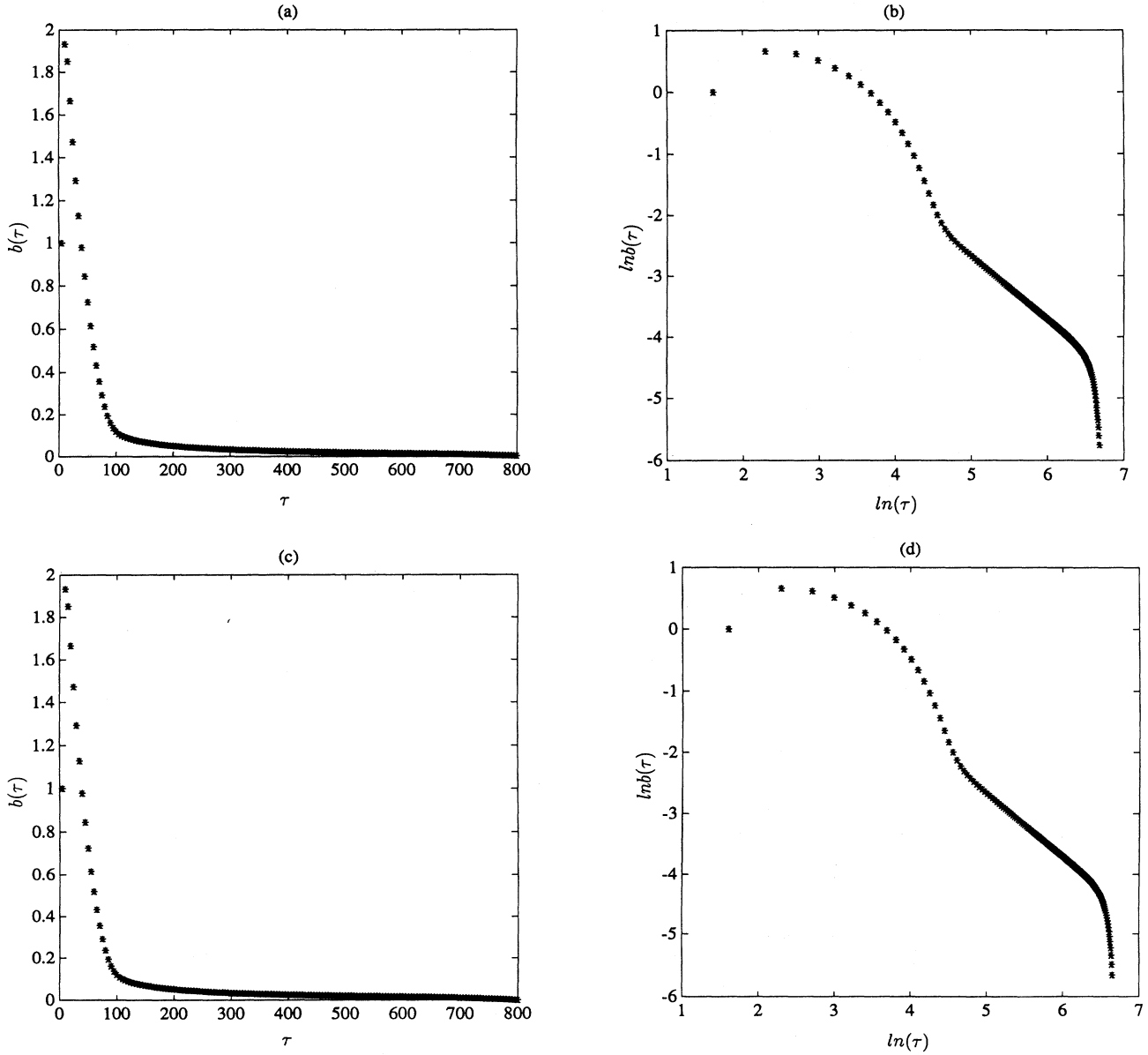

FIG. 7. The evolution of the solution from the unfiltered and filtered simulations of Eq. (1) before the first instability—extraction of $b(\tau)$ from the computed Fourier spectrum of the numerical solution: (x) computation from Eq. (12) with $n=1$; (+) computation from Eq. (12) with $n=2$. The curves overlap: (a) linear plot from the unfiltered simulation; (b) log-log plot from the unfiltered simulation; (c) linear plot from the filtered simulation; (d) log-log plot from the filtered simulation.

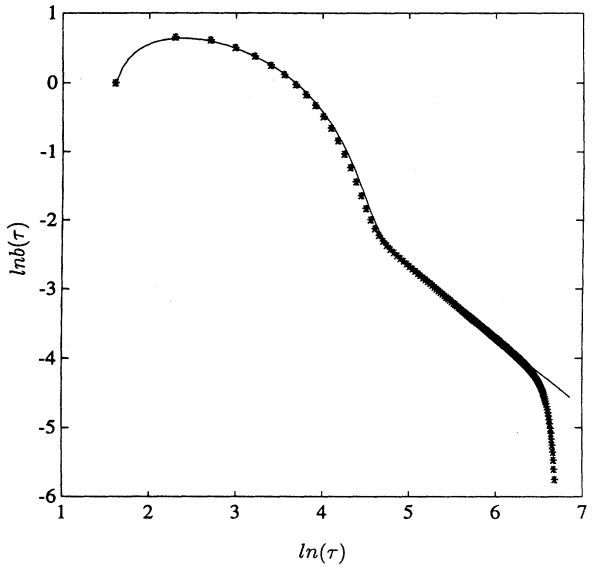

FIG. 8. Computation of $b(\tau)$: (x) from the filtered simulation of Eq. (1) as in Fig. 7, (+) from the unfiltered simulation of Eq. (1), (−) from the numerical integration of the ODE (9).

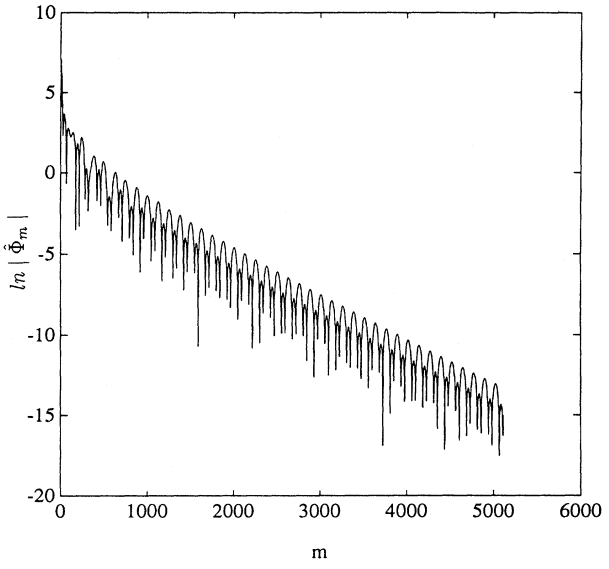

FIG. 9. The amplitude of the Fourier coefficients of the three-pole solution (13) with $b=b_1=0.01$, $b_2=0.02$ and $a_1=0.2$, $a_2=0.31$.

flame front. On the one hand, it is clear that the consideration of the previous pole solutions alone, as well as the integration of the ODEs they satisfy, is not enough for a proper answer to this question. On the other hand, our filtered numerical integrations of the PDE are certainly not noise free and the remaining round-off errors seem to play the role of the small perturbation necessary for triggering the successive instabilities observed. The resulting self-fractalization process can then be understood as a solution that successively visits various symmetric pole solutions. Before the first formation of extra cusps, we have shown that the flame interface closely follows the one-pole solution and its temporal behavior; instead, after the first instability and before the second one, the flame interface closely resembles the symmetric three-pole solution. Although a detailed, quantitative comparison has not been carried out, a good description of the flame front obtained from the integration of the PDE seems to be provided by the symmetric, exact $(2N-1)$-pole solution between the $(N-1)$th and Nth instabilities. The acceleration of the mean front radius is clearly due to these successive births of poles as the latter first go away from the real axis before approaching it again as they develop (see Figs. 7 and 8).

One may wonder whether such a fractalization process, as a whole, is computational noise. Our results show that, if this was the case, then such noise would be extremely well organized. Although we have not fully explained the entire space-time behavior, we have presented analytical expressions for the spatiotemporal structure of the solutions away from the instabilities. It would be interesting to understand and describe the space-time dynamics and its symmetries by using the approach of [14,15]. Indeed, the successive visits to the $(2N+1)$-pole analytical solutions where N increases as time evolves is similar, in a certain sense, to a uniformly traveling wave, for instance. Viewed from this perspective, the latter is nothing but the successive visits in time to various profiles which are images one of another by (spatial) translation symmetry. In the self-fractalization process studied in this paper, we anticipate that space-time symmetries also play a crucial role. They are, however, obviously different from translations. Whether they are related to space-time dilation symmetries as in the cascade process of fully developed turbulence [16] still remains an open question. The possible power-law behavior of the mean front expansion seems to indicate that this may be the case.

In addition to the fact that the self-fractalization may be related to the cascade process of turbulence, it is certainly more universal than the specific equation treated here. For instance, it has been recently reproduced in numerical integrations of a more general, geometrically invariant, model [17] for the flame dynamics in its well developed hydrodynamic instability [18].

ACKNOWLEDGMENTS

We thank R. Krasny for an interesting discussion on noise filtering techniques. Two of us (N.A. and M.R.) gratefully acknowledge the support of the National Science Foundation (NSF/PYI award No. MSS89-57462) and the Office of Naval Research, Fluid Dynamics Program (Code 1132F) (Grant No. N00014-90-J-1554). N.A. and R.L. have been collaborating under the support of NATO Grant No. 900265. G.S. gratefully acknowledges the support of the U.S. Department of Energy (Grant No. DEFG02-88ER13822), the National Science Foundation (Grant No. CTS-95-21084), and the U.S.-Israel Binational Science Foundation (Grant No. 93-00030).

[1] L. Filyand, G. I. Sivashinsky, and M. L. Frankel, Physica D **72**, 110 (1994).
[2] L. D. Landau, Acta Phys. Chem. USSR **19**, 77 (1944).
[3] G. Darrieus (unpublished).
[4] Yu. A. Gostinsev, A. G. Istratov, and Yu. V. Shulenkin, Combust. Expl. Shock Waves **24**, 70 (1988).
[5] G. Joulin, Phys. Rev. E **50**, 2030 (1994).
[6] G. Joulin, in *Combustion, Detonation, and Shock Waves,* edited by S. M. Frolov (Combustion Institute, Moscow, in press), Vol. 1.
[7] O.Thual, U. Frish, and M. Henon, J. Phys. (France) **46**, 1485 (1985).
[8] G. I. Sivashinsky, Acta Astron. **4**, 1177 (1977).
[9] G. Joulin and P. Cambray, Comb. Sci. Technol. **81**, 243 (1992).
[10] M. Renardy, Physica D **28**, 155 (1987).
[11] S. S. Minaev, Comb. Sci. Technol. (to be published).
[12] R. Krasny, J. Fluid Mech. **167**, 65 (1986).
[13] G. Hall and J. M. Watt, *Modern Numerical Methods for Ordinary Differential Equations* (Clarendon, Oxford, 1976).
[14] N. Aubry, R. Guyonnet, and R. Lima, J. Stat. Phys. **64**, 683 (1991).
[15] N. Aubry, R. Guyonnet, and R. Lima, J. Nonlinear Sci. **2**, 183 (1992).
[16] N. Aubry, R. Guyonnet, and R. Lima, J. Stat. Phys. **67**, 203 (1992).
[17] M. L. Frankel, Phys. Fluids A **2**, 1979 (1990).
[18] M. L. Frankel and G. I. Sivashinsky (unpublished).